

Nanoscale computational analysis for an idealized bio-molecular motor

R.M. PIDAPARTI^{1*}, P.W. LONGEST¹, A.T. HSU², and H.U. AKAY²

¹Department of Mechanical Engineering, Virginia Commonwealth University, Richmond, VA 23284, USA

²Department of Mechanical Engineering, Purdue School of Engineering and Technology, Indiana University-Purdue University, Indianapolis, IN 46202, USA

Abstract. Molecular motors are nature's nanomachines, and are the essential agents of movement that are an integral part of many living organisms. The supramolecular machine, called the nuclear pore complex (NPC), controls the transport of all cellular material between the cytoplasm and the nucleus that occurs naturally in all biological cells. In the presence of appropriate chemical stimuli, the NPC opens or closes, like a gating mechanism, and permits the flow of material into and out of the nucleus. As a first step in understanding the design characteristics of the NPC, nanoscale studies were conducted to understand the transport characteristics of an idealized NPC model using CFD analysis, discrete element transport and coupled fluid-solid analysis. Results of pressure and velocity profiles obtained from the models indicate that the fluid density, flexibility of walls and the geometry of the flow passage are important in the design of NPC based nano- and micro-motors.

Key words: molecular motors, atomic force microscopy, nuclear pore complex, design, simulation.

1. Introduction

Molecular motors, pumps and sorters are nature's nanomachines. They are the essential agents of movement and integral parts of many living organisms. The performance of these molecular motors, in terms of mechanical efficiency, is unparalleled by any man-made motors. Molecular motors do a variety of functions, for example, causing contraction of cardiac muscle for every heart beat, and causing the smooth muscle in our intestines to contract slowly as we digest our food. Myosins, kinesins and dyneins are best-known examples of the three families of naturally occurring motor molecules. Each family has members that transport vesicles through cell cytoplasm along linear assemblies of molecules. All these motor molecules function by undergoing shape changes utilizing energy from the biological fuel ATP (adenosine triphosphate). In contrast to single molecule motors, multi-protein complexes containing several molecules also exist in nature. The nuclear pore complex (NPC) is such a nanoscale supramolecular motor. The nuclear pore complex operates primarily via energy-dependent processes, and performs some of the most vital functions required for the survival of a cell. A nuclear pore complex, with typical dimensions of 100–200 nm, is a megadalton (MDa) heteromultimeric protein complex, which spans the nuclear envelope and is postulated to possess a transporter-containing central cylindrical body embedded between cytoplasmic and nucleoplasmic rings [1–4]. A cell has many, presumably identical, NPCs, each of which participates in the import and export of nuclear material from within the nucleus [1–3]. In the presence of appropriate chemical stimuli, the NPC opens or closes, like a gating mechanism, and permits the flow of material into and out of the nucleus. Exactly how

this transport occurs through the NPC is an open question, and a very important one, with profound implications for nanoscale devices for fluidic transport, genetic engineering and targeted drug delivery.

The NPCs are the distinctive structures of the nuclear envelope, with a molecular weight of ~ 125 MDa, and typical dimensions of 100–200 nm. The overall structure of the NPC spans the nuclear envelope with a tripartite structure consisting of a central cylindrical body embedded between cytoplasmic and nuclear octagonal rings of 32 MDa and 21 MDa, respectively [2, 4–9]. Each ring consists of eight particles positioned in a symmetrical array around a central axis spanning the cytoplasmic and nucleoplasmic surfaces of the nuclear envelope. The central body contains a channel that consists of a central granule or plug, and eight radiating spokes connecting the particles of the rings to the central granule, in a characteristic eight-fold symmetry [2, 4–9]. The central plug is a controversial component of the NPC structure [10].

Over the past few years there has been an increasing interest in the pore complex. Structural studies have been followed by elucidation of the biochemical aspects of nuclear import, and subsequent investigations into nuclear export. The current challenge is to understand the interactions between the structural elements of the pore complex and the mechanical mechanisms that drive the physical processes of translocation through it. Among the many open questions there is a need to explain the driving force exerted on a transported protein. It is expected that this force is both electrochemical and hydrodynamic in nature. We currently do not have a precise understanding of these forces, or their magnitudes. Also, the mechanical characteristics and the chemical-mechanical signal transduction are

*e-mail: rmpidaparti@vcu.edu

not known, which are critical for understanding and designing nano-scale biological motors.

Even though there are several unknowns in the transport process through this bio-molecular motor, we believe that a better understanding of mechanical and transport characteristics through computer simulation may provide us with unique solutions for designing nanoscale motors for engineering applications. We have conducted nanoscale studies involving several analyses to understand the transport characteristics of an idealized biomolecular motor. These include computational fluid dynamics (CFD) analyses of the velocity field, discrete element transport, and coupled fluid-solid interactions. The results obtained are presented to further illustrate the transport characteristics of this idealized nanoscale motor.

2. Idealized nanoscale biomolecular motor

The NPCs are distinctive structures of the nuclear envelope, with molecular weights of ~ 125 MDa, and typical dimensions of 100–200 nm. The overall structure of the NPC spans the nuclear envelope with a tripartite structure consisting of a central cylindrical body embedded between cytoplasmic and nuclear octagonal rings of 32 MDa and 21 MDa, respectively. [4–5, 13–16]. The various components making the NPC (see Fig. 1) include cytoplasm ring, central plug, spoke complex, nucleoplasmic ring, basket, and distal ring. Various components, which make up the NPC and their functions, are listed below.

Outer and inner nuclear membranes. The NPC itself is situated between the outer and inner nuclear membrane layers. The two layers are connected by supports that pass through the spoke complex [18].

Central plug. The NPC central pore (55 MDa) has 8 spokes – sandwiched between nuclear (21 Mda) and a cytoplasmic (32 MDa) rings. Fibrils emanate from the cytoplasmic ring, whereas the nuclear ring has a basket or fish trap. The central pore is sometimes referred to as a plug. There is a central channel in the plug, which is responsible for facilitated, energy-dependent, receptor-mediated nuclear transport and has a maximal size limit of around 23 nm. There are 8 peripheral channels, which account for passive diffusion of ions and small molecules [17].

Spoke complex. This is in the shape of a ring that surrounds the transporter. The outer diameter is at the inner rim of the cytoplasmic ring but at a lower level. It is a wavy ring with eight projections into the center of the NPC [18–20]. It has radial arms, which penetrate the pore membrane and project into the lumen of the nuclear envelope. The Spoke complex is sandwiched between the nucleoplasmic coaxial ring and the cytoplasmic coaxial ring.

Cytoplasmic ring. The cytoplasmic ring is made of 8 sub-units and its thickness is about 15 nm [4]. It has a diameter of ~ 120 nm and has a mass of ~ 32 MDa and stands above the level of outer nuclear membrane. It may function to hold down the Outer nuclear membrane (like a ring of eight rivets) and ensure that it connects to the pore membrane without flowing over the NPC [19]. Cytoplasmic filaments (30–50 nm long) protrude from the cytoplasmic ring of the NPC.

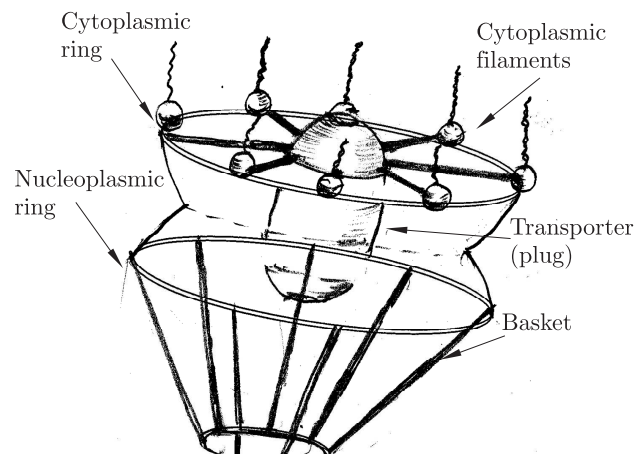


Fig. 1. A schematic of an idealized nuclear pore complex (NPC) structure

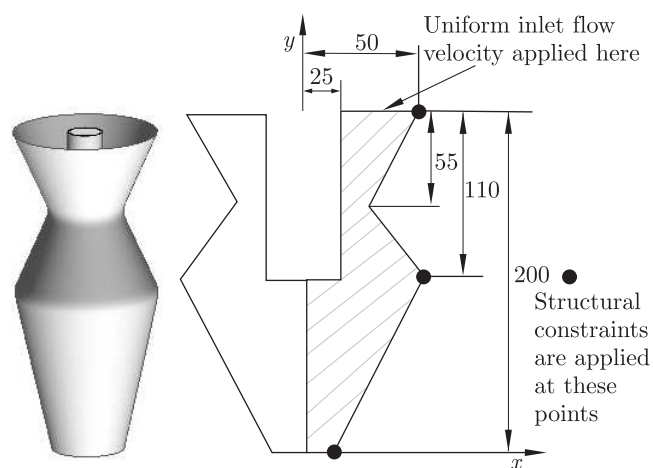


Fig. 2. Surface model and geometric details of an idealized simulation model of NPC (all dimensions are in nm)

Nucleoplasmic ring. Nucleoplasmic rings have sub-units, which are triangular in shape. They are very different from the cytoplasmic ring subunits, which are bipartite and much thicker [18]. The nucleoplasmic face of the NPC also exhibits 50–100 nm long filaments that extend from the nucleoplasmic ring, and are joined distally by a 30–50 nm diameter terminal ring, forming a basket structure.

Basket. It is the initial contact site for the export cargo and also the termination site for the import process. It may act as “waiting station” or “staging area” for large RNP’s to be exported. It holds the NPC in place by attaching to the nuclear lamina [17,18]. It has filaments which are ~ 10 nm diameter and are attached to the outer periphery of the nucleoplasmic ring, at a position between two subunits, which stand independent of the level of the inner nuclear membrane. Each filament extends into the nucleoplasm and branches at its distal end [20].

Distal ring. The Distal ring is a part of the basket assembly and studies have shown that it acts as a filter and is formed during the export of molecules from the nucleus to the cytoplasm.

An idealized model of NPC containing the central plug, bottom basket and top cytoplasm rings, similar to the one described in the literature [4], were considered. The idealized configuration of the NPC is shown in Fig. 2.

3. Materials and methods

As a first step in understanding the transport characteristics of the NPC, preliminary studies were conducted using CFD analysis, discrete element transport, and coupled fluid-solid analysis to understand the fluid dynamics characteristics of the NPC model. The inclusion of fluid-structure interactions is expected to be a critical component in the functioning of the NPC and the development of similar nanomachines. The scale of the flow field is on the order of 100 nm. For liquid flow, this represents a largely continuous regime with non-continuum variations at the walls. However, these non-continuum effects are largely a function of wall surface properties, which are not currently available. As such, the no-slip boundary condition has been employed as a first-order approximation. This and other assumptions are not expected to have a significant impact on the fluid-structure effects of this preliminary study.

Idealized computational model. A two-dimensional axisymmetric model of an idealized NPC containing the three essential structural elements, i.e., the central plug, bottom basket and top cytoplasm rings, is considered in this study (Fig. 2). This is an approximate model of the actual NPC but includes three important nanostructural components of the NPC. The purpose of this model is to determine the role of the central plug in relation to the outer wall (rigid as well as deformable) on velocity and pressure variations in the NPC. Fluid and structural properties of the NPC elements are not known, but some studies suggest that it is like a cellular material, hence material properties of cells from the existing experimental data [10–12] are used. The working fluid in the NPC is cellular cytoplasm, which is composed primarily of water. For this analysis, the internal fluid has been assumed to be water with properties taken at 37°C.

CFD analysis. Computational evaluation of the NPC-based structure requires solving the governing conservation equations for mass and momentum, as shown below for incompressible laminar biofluid flows [21]:

$$\nabla \times \vec{u} = 0 \quad (1)$$

$$\frac{\partial \vec{u}}{\partial t} + (\vec{u} \times \nabla) \vec{u} = \frac{1}{\rho} \left(-\nabla p + \nabla \times \vec{\tau} \right) \quad (2)$$

where \vec{u} is the velocity vector, p is the pressure, ρ is the fluid density, the shear stress tensor is given by

$$\vec{\tau} = \mu \left[\nabla \vec{u} + (\nabla \vec{u})^T \right] \quad (3)$$

and μ is the absolute viscosity.

The above equations are for a stationary mesh and continuum flow. Details of the fluid-structure coupling algorithm are provided below. For liquid flow in a 100 nm structure, noncontinuum effects will become significant and must be accounted

for using correction models. For liquid flow, the no-slip boundary condition will be assumed valid at the wall [22]. However, electrostatic, surface tension, and surface roughness effects may be considered in future studies. Electrostatic forces and surface tension can be modeled directly [22,23]. To address surface roughness, near-wall porous media and roughness viscosity models will be employed [24,25].

Discrete element transport. Evaluation of the sorting characteristics of the simplified NPC-based structure shown in Fig. 1 requires tracking discrete elements and predicting their interaction with the inner and outer walls. For sufficiently small discrete elements and perfect wall absorption, the continuum equation for dilute chemical species may be used. However, this methodology is not capable of predicting the wall and fluid interactions of the 5–20 nm discrete elements of interest here. Alternately, a model based on Newton's Second Law that can be used to approximate particle wall interactions and can be expressed as [26]

$$\frac{dv_i}{dt} = \frac{f_d}{\tau_p C_c} (u_i - v_i) + f_{i,near-wall} + f_{i,brown} + f_{i,turb} + f_{i,electrostatic} \quad (4a)$$

$$\frac{dx_i}{dt} = v_i(t) \quad (4b)$$

In the above equations, v_i and u_i are the components of the particle and local fluid velocity, respectively. The characteristic time required for particles to respond to changes in the flow field, or the momentum response time, is $\tau_p = \rho_p d_p^2 / 18\eta$. The first term on the right hand side of Eq. (4a) represents particle drag including the Cunningham correction factor for molecular slip. The drag coefficient f_d for rigid and deformable particles is available from Clift et al. [27]. For the extremely low Stokes numbers of interest in this geometry, Stokes drag was assumed, which is represented as $f_d = 1$. Brownian motion, which arises from molecular collisional effects on small particles and results in diffusion, is represented as a stochastically fluctuating force with zero mean and a 3-D variance of $6Dt$ where D is this diffusion coefficient available from the Stokes-Einstein equation [29]. Calculation of the near-wall forces has been described in Longest et al. [28].

To solve the equations governing fluid flow and discrete element transport, a commercial CFD package (FLUENT) was used. This commercial software provides an unstructured control-volume-based solution method for multiple mesh styles including structured hexahedral, unstructured tetrahedral, and hybrid meshes. User-supplied Fortran and C programs have been employed for the calculation of initial particle profiles, particle deposition locations, grid convergence, and post processing. All transport equations were discretized to be at least second order accurate in space. For the convective terms, a second order upwind scheme was used to interpolate values from cell centers to nodes. The diffusion terms were discretized using central differences. Nodal values for the computation of gradients were constructed from the weighted average of the surrounding cells. A segregated implicit solver

was employed to evaluate the resulting linear system of equations. This solver uses the Gauss-Seidel method in conjunction with an algebraic multigrid approach to solve the linearized equations. The SIMPLIC algorithm was employed to evaluate pressure-velocity coupling. The outer iteration procedure was stopped when the global mass residual had been reduced from its original value by five orders of magnitude and when the residual-reduction-rates for both mass and momentum were sufficiently small. To ensure that a converged solution had been reached, residual and reduction-rate factors were decreased by an order of magnitude and the results were compared. The stricter convergence criteria produced a negligible effect on both velocity and particle deposition fields. In order to resolve the extremely small scales of interest, non-dimensional scaling of the system was implemented, along with double precision calculations. Specifically, the geometry was scaled by a factor of 10^6 and the Stokes, Reynolds and Peclet numbers were matched to their original values.

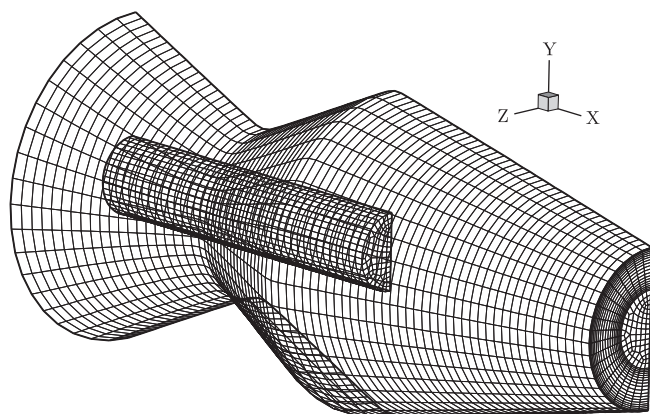


Fig. 3. Hexahedral computational grid for CFD analysis

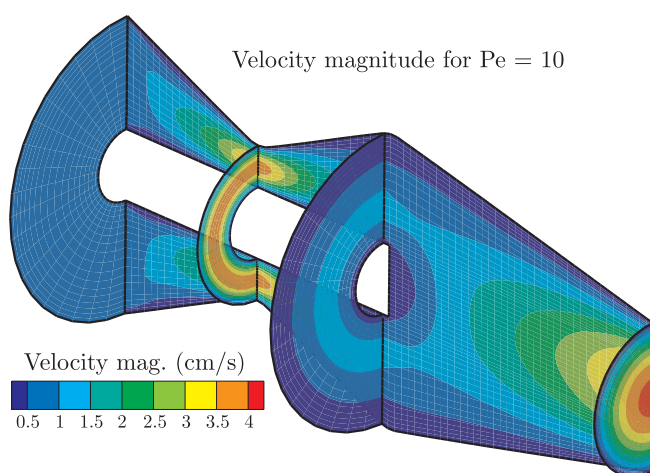


Fig. 4. Velocity magnitude for a uniform velocity inlet of 0.6 cm/s

Coupled fluid-solid analysis. An idealized two-dimensional model of NPC is developed and analyzed with ANSYS software. A coupled field analysis is performed on the model by taking the interaction between the fluid and solid parts. The fluid part is solved using the FLOTTRAN solver of

ANSYS, the impact of which on the structure is determined with the coupling of two media. The analysis is performed sequentially by solving the fluid media first using the FLOTTRAN macro of ANSYS. The pressure loads from the fluid are in turn applied on the structure, which deforms under the fluid pressures. As a result, the fluid mesh is updated based on the structural deformation and this is carried in an iterative manner until the equilibrium (which is specified by the user) is reached. FSSOLV macro provided by ANSYS, was used to perform the analysis. When the solid part is assumed rigid, the interaction is ignored and only the flow analysis is performed.

Two different analyses models, one with rigid walls and one with flexible walls, were developed and investigated to study the fluid dynamics characteristics and comparisons between them. The results of pressures and velocities obtained from these models are presented and discussed under different geometric parameters. Figure 2 shows the geometric and analysis model details considered in this study. The analysis model consists of Fluid 141 (2D fluid elements), and Plane 42 (2D structural elements) in the ANSYS finite element software. The idealized model consisted of 830 structural elements and 1133 fluid elements. The shaded portion is considered for the analyses. Due to the symmetry of the model about the y -axis, only a half section of the model is analyzed. Structural properties based on existing experimental data [10–12] for the NPC walls include a Young's Modulus of 1.0×10^6 Pa and a Poisson's ratio of 0.45. The outer wall was constrained in both x - and y -directions at three points and along the length of the plug as shown in Fig. 2. From the coupled fluid-solid analysis, results of pressure and velocity contours as well as structural displacements are obtained.

4. Results and discussion

The hexahedral computational grid used to discretize the flow field equations is shown in Fig. 3. The inner core of the geometry was meshed using a hexahedral-Cooper style. This structure was surrounded by a multiblock structured mesh. Hexahedral elements were selected based on their improved accuracy, especially when applied to near-wall particle tracking [26].

Velocity magnitude at the midplane and selected cross-sectional locations is shown in Fig. 4 for a uniform input velocity of 0.6 cm/s (un-scaled) and an inlet Reynolds number of 10^{-4} . Due to the dominate viscous forces, the flow profiles are largely parabolic and fully developed at all locations. Separation and recirculation were not observed in the flow field. However, the geometry variation did have a significant impact on the velocity and pressure distribution in the region of the constriction.

As a case study, 10 nm particles were initialized uniformly over the inlet and tracked under steady flow conditions. A Peclet number to describe the discrete phase can be defined as $Pe = VL/\Delta$ where V and L represent the characteristic velocity and diameter of the simplified NPC-based structure, and Δ is the diffusion coefficient of the discrete elements. As such, the Peclet number defined above represents the ratio of convective fluid motion to particle diffusion. Particles have been

assumed to be spherical and non-hydrated, and the Stokes-Einstein relation has been used to estimate particle diffusivity.

Simulations of particle trajectories for $Pe = 1$ (diffusion dominant flow) indicate that random particle motions result in wall contacts for all particles in the upstream region of the geometry (Fig. 5a). As convective forces are increased ($Pe = 100$) random motions remain largely evident along the particle tracts. However, some particles are able to escape the geometry without contacting the wall surface (Fig. 5b). For convection dominated flows ($Pe = 10,000$) a much smaller fraction of particles contacts the NPC wall (Fig. 5c).

Deposition locations shown in Fig. 6 indicate that particles with lower Peclet numbers rapidly deposit on the upstream portion of the NPC-based structure. As the Peclet number is increased, deposition fractions are reduced and deposition locations are shifted downstream. Deposition fractions for a range of Pe values (0.1–10,000) are shown in Fig. 7. A significant finding highlighted in this figure is the occurrence of an effective cutoff Peclet number for particle deposition. For Pe less than 10, most particles are captured by wall deposition. For Peclet numbers greater than approximately 10, there is an exponential decrease in the number of particles interacting with the wall. This finding may have significant implications with respect to designing NPC-based filtering and sorting structures.

In order to see how the fluid is transported in the idealized NPC model, several finite element runs were carried out and the results of velocity and pressures are obtained. Figure 8 shows the velocity vector plot comparison of rigid walls versus deformable walls models. We can see from the figure that the maximum velocity in both cases is attained in the constricted region (throat), but the magnitude of velocity obtained from only the flow analysis is more than that of the one obtained from coupled-field analysis. Figure 9 shows the comparison of pressures between the two analysis models. We can see that the magnitude of the velocity in the throat area is more in the model with rigid walls than that of the other model with deformable walls, as can be seen by the longer arrows.

Figure 10 shows the plot of the pressure and velocity ratios (defined as the ratio of maximum pressure or velocity at the throat obtained from the rigid-wall model to those from the deformable-wall model) along the length of the throat defined by a non-dimensional x -distance from the plug surface normalized with respect to throat width. We can see that there are velocity and the pressure gains when the model is analyzed using just the fluid analysis with rigid walls. The loss of velocity and pressure in the coupled-field analysis is attributed to the deformation of the walls. Figure 11 shows the pressure variation along the outer wall boundary from the two analysis models. It can be seen that the pressure distribution is similar, but the magnitudes are much different when the walls are flexible. Figure 12 shows the effect of the pressure exerted by the fluid on the structure. It can be seen that the structural displacements are quite substantial. This is an important aspect, since the flexible wall of the motor may be responsible in transporting both large and small molecules through the NPC by going through wall deformations.

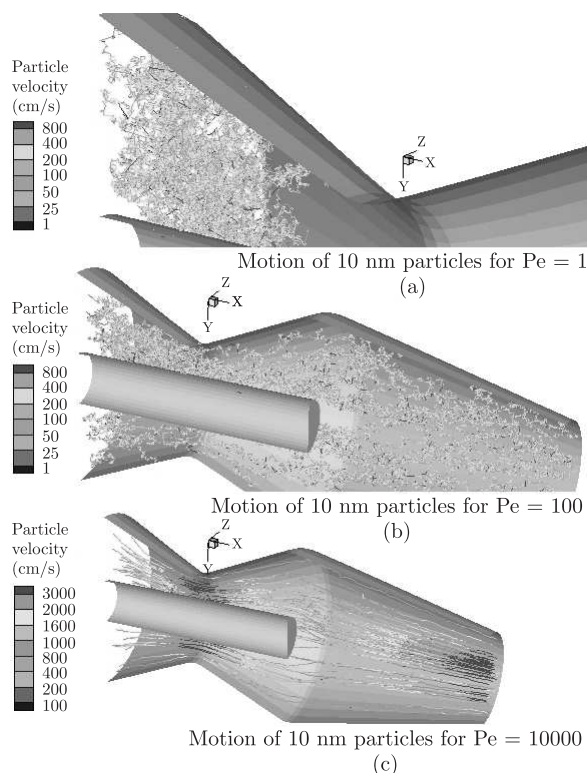


Fig. 5. Particle trajectories through the NPC for $Pe = 1$ (a); $Pe = 100$ (b); $Pe = 10,000$ (c)

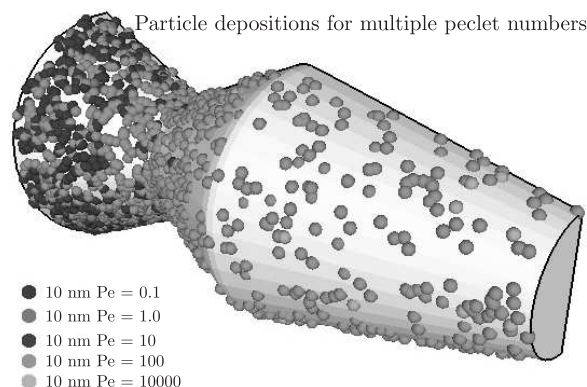


Fig. 6. Internal particle deposition locations for 10 nm particles at various Peclet numbers

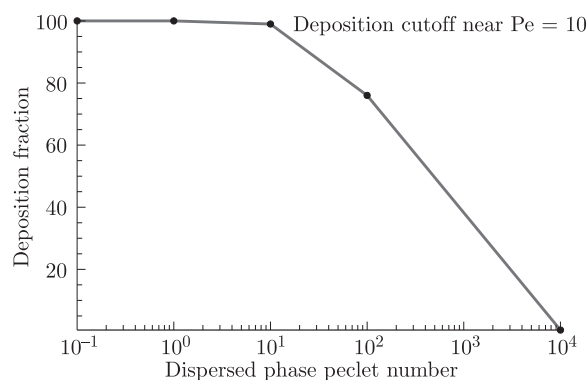


Fig. 7. Deposition fraction vs. Peclet number

R.M. Pidaparti, P.W. Longest, A.T. Hsu, and H.U. Akay

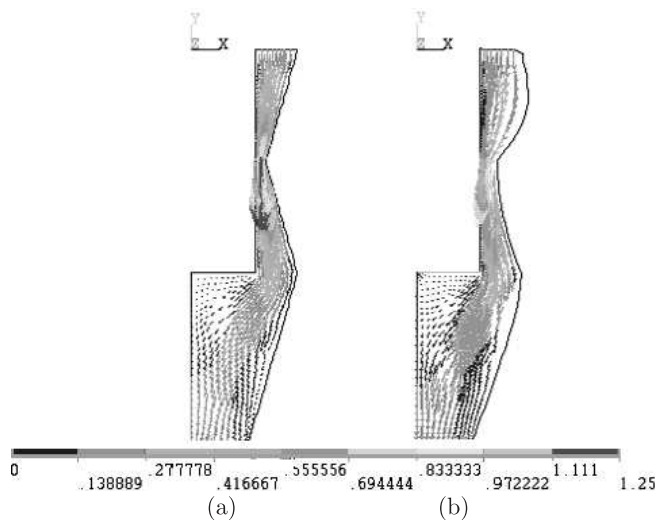


Fig. 8. Velocity vectors flow analysis (a), coupled-field analysis (b)

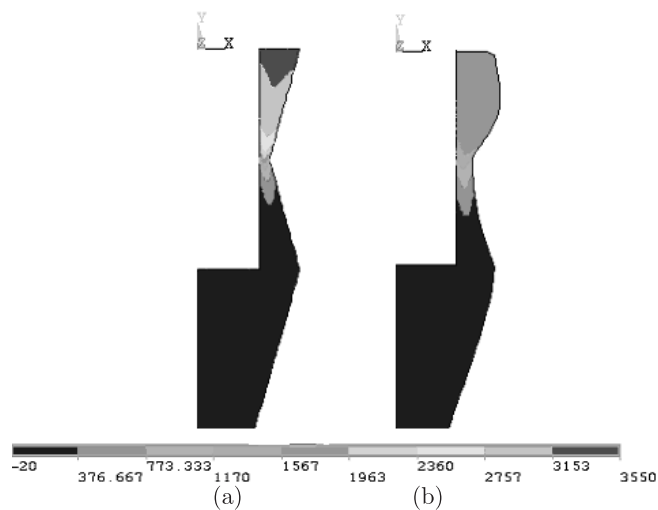


Fig. 9. Comparison of pressure flow analysis (a), coupled-field analysis (b)

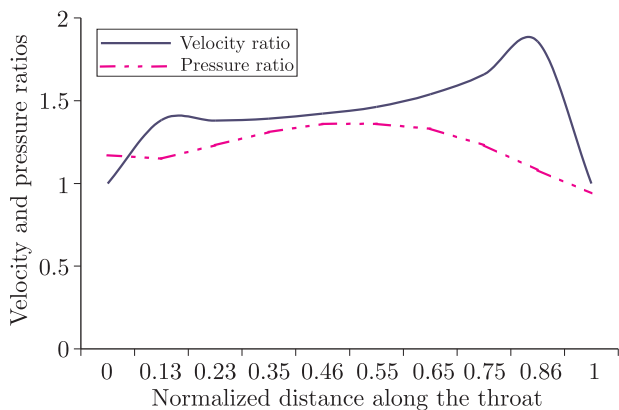


Fig. 10. Plot of Pressure and velocity ratios for comparison of rigid-wall versus deformable-wall models

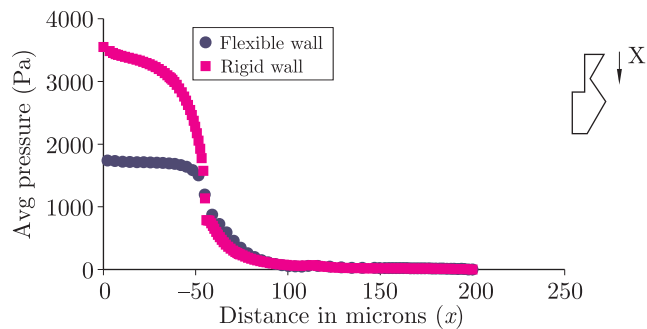


Fig. 11. Plot of pressure along the wall boundary for rigid-wall versus deformable-wall models

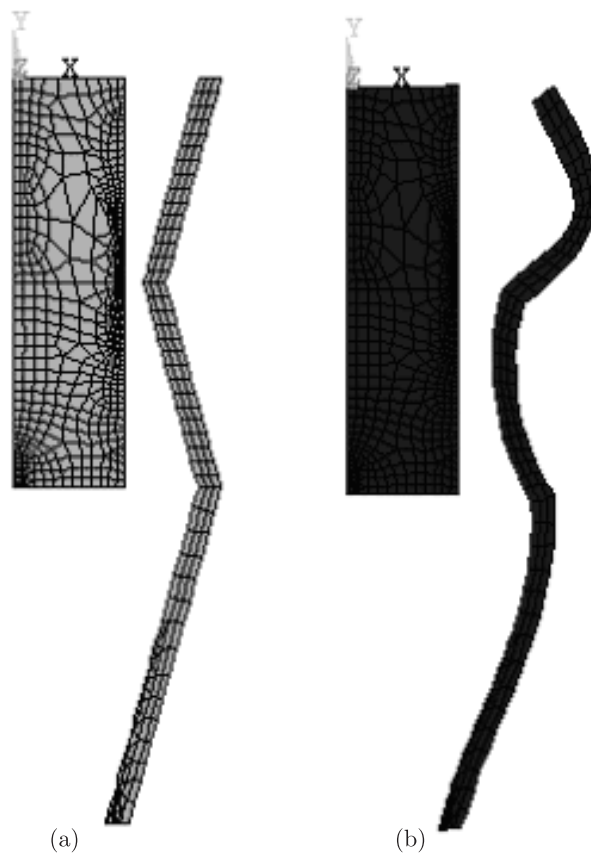


Fig. 12. Structural deformation of the wall of the NPC model rigid wall (a), flexible wall (b)

Design analysis. Figure 7 provides an example of the design analysis that can be performed based on the results of this study. In Fig. 7, a cutoff value of $Pe = 10$ is observed, below which particles typically hit the wall and are trapped. Depending on the properties of the particles to be transported, NPC structures can be designed to either trap or filter discrete elements. For instance, a hypothetical design objective may be to trap particles less than 50 nm. The associated diffusion coefficient for these particles is $1.0e-7 \text{ cm}^2/\text{s}$. To produce a Peclet number less than 10, the product of velocity and inlet diameter must be less than $1.0e-6 \text{ cm}^2/\text{s}$. For the 100 nm structured considered, the resulting inlet velocity of the system required

to trap nearly all particles less than 50 nm should be 0.1 cm/s or less.

In order to determine how the length and diameter of the plug may affect the pressure and velocity profiles, five cases of coupled field analysis were run with different L (plug length) /D (throat width) values. The results indicate that when the ratio of L/D is increased about two times, the velocity at the throat decreases by 40% and decreases after that. Similarly, the pressure increases about 180% when the L/D ratio is increased from 1.375 to 2.75 and after that the pressure decreases. These results indicate that L/D ratio is an important parameter in controlling the fluid behavior through NPC.

The NPC regulates large as well as small molecules in the transport process. High concentration slurries of molecules at very low Reynolds numbers can be assumed to behave as a homogeneous mixture with modified properties. This scenario was simulated in the model by simulating a case with high and low fluid densities. The results obtained by changing the fluid density indicate that fluid pressures increase by about 70% when the fluid density is increased by four times. Even though there is not much change in the velocity, there is a 100% change in the wall deformation when the fluid density is increased by four times. These results indicate that fluid density mimicking the large and small molecules may play a role in controlling the transport.

5. Concluding remarks

Several nanoscale studies using CFD analysis, discrete element transport and coupled fluid-solid analysis were carried out to understand the transport characteristics of the idealized NPC model. As expected, the flow field of the idealized structure was nearly parabolic and fully developed at all locations. Flow separation and recirculation were not observed. With respect to particle deposition, an effective cutoff value for the Peclet number was observed at Pe_{10} , below which all particles deposited on the wall. It was found that the effect of flexible walls, L/D ratios and fluid density strongly influence the pressure distributions. The results obtained also indicate that for a realistic analysis, coupled fluid-solid analysis is necessary. Results of pressure and velocity profiles obtained from the models indicate that the fluid density, flexibility of walls and the geometry of the flow passage are important in the design of NPC based nano- and micro-motors. Even though this model has certain limitations in terms of the assumption employed, the fluid dynamics behavior obtained from this study on an idealized NPC will help to gain further clues for more interesting and biologically inspired designs. A refined model of the NPC is under investigation, and results from continuum as well as non-continuum correction methods will be compared in the future.

Acknowledgements. The authors thank Drs. Frank Prendergast and Marc Gacy of Mayo Clinic for their help and support in the course of this study. The first author thanks Drs. Gautam Vemuri and Sarma Pidaparathi of Indiana University-Purdue University Indianapolis for their help and discussions.

The solid-fluid interaction modelling help provided by Mr. Viswanath Someshekar is acknowledged.

REFERENCES

- [1] N. Thomas and R.A. Thornhill, "The physics of biological molecular motors", *J. BioPhysics* 386, 253–266 (1998).
- [2] H.C. Taylor and M.E.J. Holwill, "Axonemal dynein – a natural molecular motor", *J. Nanotechnology* 10, 237–243 (1999).
- [3] C.W. Akey and M. Radmacher, "Architecture of the xenopus nuclear pore complex revealed by three-dimensional cryo-electron microscopy", *J. Cell Biol.* 122, 1–19 (1993).
- [4] N. Pante and U. Aebi, "Towards understanding the 3-D structure of the nuclear pore complex at the molecular level", *Curr. Opin. Struct. Biol.* 4, 187–196 (1996).
- [5] C.W. Akey, "Interactions and structure of the nuclear pore complex revealed by cryo-electron microscopy", *J. Cell Biol.* 109, 955–970 (1989).
- [6] J.A. Hanover, "The nuclear pore at the crossroads", *FASEB J.* 4, 187–196 (1992).
- [7] N. Pante and U. Aebi, "Sequential binding of import ligands to distinct nucleopore regions during their nuclear import", *Science* 273, 1729–1732 (1996).
- [8] H.W. Wang and D.E. Clapham, "Conformational changes of the in situ nuclear pore complex", *J. Biophysical* 77(1), 241–247 (1999).
- [9] U.F. Greber and L. Gerace, "Depletion of calcium from the lumen of endoplasmic reticulum reversibly inhibits passive diffusion and signal-mediated transport into the nucleus", *J. Cell. Biol.* 128, 5–14 (1995).
- [10] C. Perez-Terzic, J. Pyle, M. Jaconi, L. Stehno-Bittel, and D. Clapham, "Conformational states of the nuclear pore complex induced by depletion of nuclear Ca^{2+} stores", *Science* 273, 1875–1877 (1996).
- [11] C. Perez-Terzic, A.M. Gacy, R. Bortolon, P.P. Dzeja, M. Puceat, M. Jaconi, F.G. Prendergast, and C.A. Terzic, "Structural plasticity of the cardiac nuclear pore complex in response to regulators of nuclear import", *Circ. Res.* 84, 1292–1301 (1999).
- [12] C. Perez-Terzic, M. Jaconi, and D.E. Clapham, "Nuclear calcium and the regulation of the nuclear pore complex", *BioEssays* 19, 787–792 (1997).
- [13] L. Pemberton, G. Blobel, and J. Rosenblum, "Transport routes through the nuclear pore complex", *Curr. Opin. Cell Biol.* 10, 392–399 (1998).
- [14] T.M. Gant, M.W. Goldberg, and T.D. Allen, "Nuclear envelope and nuclear pore assembly, analysis of assembly intermediates by electron microscopy", *Curr. Opin. Cell Biol.* 10 (3), 409–15 (1998).
- [15] N. Pante and U. Aebi, "Molecular dissection of the nuclear pore complex", *Critical Reviews in Biochemistry and Molecular Biology* 31(2), 153–99 (1996).
- [16] D.D. Newmeyer, "The nuclear pore complex and nucleocytoplasmic transport", *Curr. Opin. Cell Biol.* 5(3), 395–407 (1993).
- [17] T.D. Allen, J.M. Cronshaw, S. Bagley, E. Kiseleva, and M.W. Goldberg, "The nuclear pore complex: mediator of translocation between nucleus and cytoplasm", *J. Science* 113, 1651–1659 (2000).
- [18] M.W. Goldberg and T.D. Allen, "The nuclear pore complex and lamina: three-dimensional structures and interactions determined by FEISEM", *J. Mol. Biol.* 257, 848–865 (1996).
- [19] M.W. Goldberg and T.D. Allen, "Structural and functional organization of the nuclear envelope", *Curr. Opin. Cell Biol.* 7, 301–309 (1995).

- [20] E. Kiseleva, M.W. Goldberg, T.D. Allen, and C.W. Akey, "Active nuclear pore complexes in Chironomus: visualization of transporter configurations related to mRNP export, *J. Cell Science* 111, 223–236 (1998).
- [21] P.W. Longest and C. Kleinstreuer, "Comparison of blood particle deposition models for non-parallel flow domains", *J. Biomechanics* 36(3), 421–430 (2003).
- [22] G.E. Karniadakis and A. Beskok, *Microflows: Fundamentals and Simulation*, Springer Verlag, New York, 2002.
- [23] M. Gad-el-Hak, *The MEMS Handbook*, CRC Press, New York, 2002.
- [24] J. Koo and C. Kleinstreuer, "Liquid flow in microchannels: experimental observations and computational analyses of microfluidics effects", *J. Micromech. Microeng.* 13, 568–579 (2003).
- [25] G.M. Mala and D. Li, "Flow characteristics of water in microtubes", *International J. Heat and Fluid Flow* 20, 142–148 (1999).
- [26] P.W. Longest, C. Kleinstreuer, and J.R. Buchanan, "Efficient computation of micro-particle dynamics including wall effects", *Computers & Fluids* 33 (4), 577–601 (2004).
- [27] R. Clift, J.R. Grace, and M.E. Weber, *Bubbles, Drops, and Particles*, Academic Press, New York, 1978.
- [28] C. Crowe, M. Sommerfeld, and Y. Tsuji, *Multiphase Flows with Drops and Bubbles*, CRC Press, Boca Raton, 1998.